Sacrificial Anode Cathodic Polarization of Steel in Seawater: Part 1 — A Novel Experimental and Analysis Methodology

*W. Wang, W.H. Hartt, and S. Chen**

ABSTRACT

API-2H, grade 42 steel (UNS K12037) specimens were cathodically polarized in natural seawater by galvanic coupling to an aluminum anode through an external resistor. The interdependence of the decay in potential (ϕ) vs current density (i) conformed analytically to a straight line, the slope of which was the product of the total circuit resistance and cathode surface area and the vertical intercept of which was the anode corrosion potential. From experiments with resistor sizes ranging from 75 Ω to 5,750 Ω, a sigmoidal shape for the curve defining the relationship between long-term ϕ and i values for cathodically polarized steel in seawater was identified, with –1.00 V_{SCE} being the potential of minimum steady-state (maintenance) current density (i_m). Evaluation of data from instrumented, newly deployed offshore structures and of survey data from older structures indicated that the ϕ-vs-i trend for these structures conformed to the same linear relationship as the laboratory specimens. A procedure was developed whereby polarization data from systems of vastly different geometries can be interrelated quantitatively.

KEY WORDS: calcareous deposits, cathodic polarization, cathodic protection, marine environments, offshore structures, sacrificial anode, seawater, structural steel

INTRODUCTION

Cathodic protection (CP) has been the fundamental means of corrosion control for submerged marine structures for several decades. While several criteria for defining the adequacy of CP are available, a requirement of polarization to –0.80 $V_{Ag\text{-}AgCl}$ or more negative is widely used and specified.[1-2] CP system designs to achieve this potential have been based up until about the last decade upon a single requisite current density (i), the magnitude of which was a function of water properties (temperature, wave action, and flow conditions). The lowest i value that was considered to result in adequate polarization in the long term was used. Thus, protection typically would be inadequate initially, but the level of polarization would reach an acceptable level after several months to a year.

Cox[3] demonstrated more than 50 y ago that the application of a relatively high i value initially resulted in formation of calcareous deposits[4-10] that were particularly protective and that yielded a lower maintenance or long-term current density (i_m) than if a relatively low initial i value was used with more gradual polarization. Based upon laboratory data, service data, or both, various investigators have revisited the high initial i-value approach (alternately termed rapid polarization);[11-14] and this technology now is used routinely for CP system design of offshore petroleum production structures. The concept of rapid polarization appears to contradict the generally recognized relationship between potential (ϕ) and i value, where the former becomes more negative as the latter increases. This is explained in terms of formation in the –0.90 V to –1.00 V potential range of a particularly protective calcareous deposit. Figure 1 shows schematically the long-term ϕ-vs-i relationship that generally is acknowledged to prevail.

In an attempt to quantify the above polarization behavior, Fischer, et al., considered the interrelation-

Submitted for publication February1995.
* Center for Marine Materials, Florida Atlantic University, P.O. Box 3091, Boca Raton, FL, 33431-0091.

0010-9312/96/000093/$5.00+$0.50/0
© 1996, NACE International

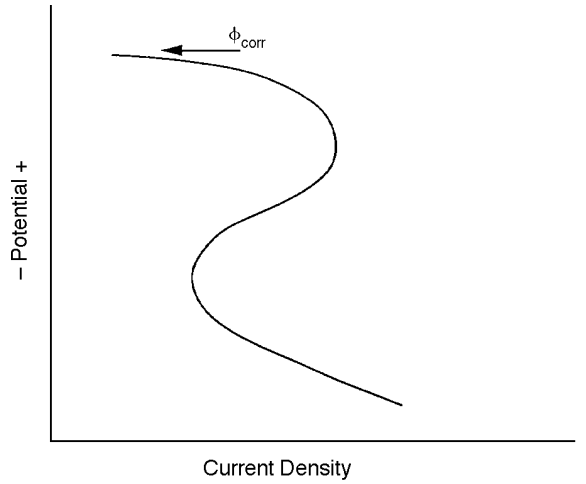


FIGURE 1. *Schematic of the steady-state cathodic polarization curve for steel in seawater (ϕ_{corr}, corrosion potential).*

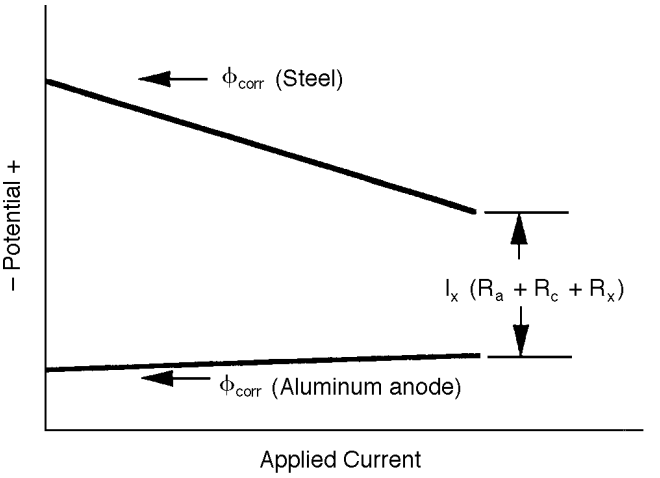


FIGURE 2. *Schematic of the polarized state of a steel cathode and anode in seawater.*

ship between the polarized anode and cathode potentials (ϕ_a and ϕ_c, respectively) in terms of the anodic or cathodic current (I_a or I_c, respectively) according to Ohm's law as:[14]

$$I_a = I_c = \frac{\phi_c - \phi_a}{R_x + R_c + R_a} \quad (1)$$

where R_x, R_c, and R_a are the external (metallic path), cathode and anode resistances, respectively. This situation is represented in terms of the schematic polarization diagram in Figure 2. Equation (1) may be rewritten as:

$$\phi_c = \left(R_x + R_c + R_a\right) I_c + \phi_a \quad (2)$$

from which the dependence of ϕ_c upon I_c is seen to be linear, assuming that the resistance terms and ϕ_a are constant. Recognizing that:

$$I_c = i_c \times A_c \quad (3)$$

where i_c is the cathodic current density, and A_c is the cathode area, and

$$R_t = R_x + R_c + R_a \quad (4)$$

where R_t is the total circuit resistance, then:

$$\phi_c = \left(R_t \times A_c\right) i_c + \phi_a \quad (5)$$

Thus, the slope of the linear interdependence between ϕ_c and i_c is projected to be the product of the total circuit resistance and A_c with the vertical axis intercept corresponding to ϕ_a. Although the limited data developed by Fischer, et al., from field exposures were mixed with regard to confirming the appropriateness of Equation (5),[14] Wolfson noted such confirmation based upon laboratory and field tests.[15] If this is the case, then a technique may exist to conveniently quantify ϕ-vs-i interrelationships associated with sacrificial-anode CP. This, in turn, may have utility with regard to CP survey data analysis and the design of new and retrofit CP systems.

The objectives of the present research were to define the extent to which Equation (5) is accurate and useful and, where appropriate, to develop a methodology to represent and correlate laboratory and in-service CP system performance.

EXPERIMENTAL PROCEDURE

The experimental program used a cylindrical cathode (25.4 mm [1 in.] diameter by 50.8 mm [2 in.] high) of API-2H,[(1)] grade 42 steel (UNS K12037),[(2)] the composition of which is reported in Table 1. The anode was machined from a commercial 330-kg (725-lb) aluminum-zinc-mercury anode to a rectangular cross-section ring geometry with outside diameter of 57.2 mm (2.25 in.), inside diameter 44.5 mm (1.75 in.), and thickness 3.2 mm (0.13 in.). Table 2 provides the chemical composition for this electrode. The cathode was mounted using a polytetrafluoroethylene (PTFE) holder that sealed the circular top and bottom faces such that the exposed surface area was ≈ 40.5 cm^2 (6.28 in.^{2}). The anode ring (surface area 29.8 cm^2 [4.6 in.^{2}]) was positioned symmetrically in the cell about the cathode. Electrical connection of the two electrodes to one another included an exter-

[(1)] American Petroleum Institute, 1220 L St., NW, Washington, DC, 20005.

[(2)] UNS numbers are listed in *Metals and Alloys in the Unified Numbering System*, published by the Society of Automotive Engineers (SAE) and cosponsored by ASTM.

TABLE 1
Composition of the Cathode Test Material (API-2H, Grade 42 Steel)[A]

C	Si	Mn	P	S	Cu	Ni	Cr	Mo	V	N
0.09	0.33	1.54	0.02	0.003	0.24	0.4	0.03	0.003	0.005	0.0026

[A] Balance Fe.

nal resistor, the magnitude of which ranged from 75 Ω to 5,750 Ω. This resistor provided a means for current measurement and to limit the magnitude of polarization for the cathode according to a predetermined amount and, as such, permit simulation of a more extreme surface area ratio (smaller anode-to-cathode) than was actually the case. Voltage drop across the external resistor and cathode potential were measured, the latter using a commercial saturated calomel electrode (SCE), and recorded by a personal computer-based data acquisition system at time intervals ranging from 10 s to 2 h.

The test cells consisted of a series of 2-L (2.1-qt) polymethyl methacrylate (PMMA) cylinders (Figure 3). The reference electrode (RE) was connected to the instrumentation on the cathode side of the external resistor. Independent measurements with a probe confirmed that the recorded values were independent of its position and of the presence of the anode. The electrolyte was once-through natural seawater, the properties of which have been reported previously.[16] Flow rate through the cells was 150 mL/min, and the temperature was 23°C to 25°C.

RESULTS AND DISCUSSION

Polarization Data Analysis

More than 150 experiments were performed according to the procedure detailed above. Of these, Figures 4(a) through (c) present typical results as plots of ϕ_c vs time, i_c vs time, and ϕ_c vs i_c (subsequently termed the ϕ-vs-i decay diagram) for the specific case of R_x = 149 Ω (R_t x A_c = 0.60 Ω-m^2 assuming $R_t = R_x$). For the last of these representations (Figure 4[c]), data corresponding to the initial exposure are at the upper right, and the progression with time is to the lower left. Figure 5 illustrates this schematically with three regions being identified. In the first (Region 1), which corresponds to the initial exposure, current density increased and potential became more negative with time (note the extreme upper right of the data in Figure 4[c]). The period for this behavior typically lasted for several minutes only. Subsequently, both potential and current density decreased with time according to a linear trend (Region 2). After ~ 400 h, however, ϕ_c drifted between –1.03 V_{SCE} and –0.96 V_{SCE}, while i_c decreased continuously and, after ≈ 1,700 h, reached an apparent steady-state value (equivalent to i_m).[1] This regime of potential drift defined Region 3.

TABLE 2
Composition of Anode Test Material[A]

Zn	Fe	Si	Hg	Cu
1.3	0.05	0.05	0.046	0.0015

[A] Balance Al.

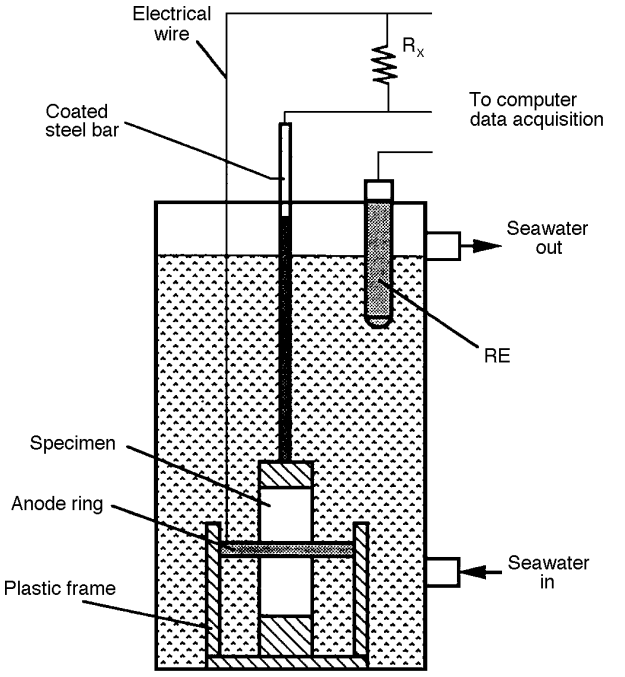


FIGURE 3. *Test cell setup.*

It was projected that Equation (5) applies universally and describes the behavior in all three regions. That the data conformed to a linear trend in Region 2 only was consistent with R_t and ϕ_a being constant. The lack of linearity in Regions 1 and 3 indicated one or both of these parameters apparently was time-dependent during these periods.

The trend in Region 1 was consistent with activation of the anode and a shift in its potential to a more negative value (variable ϕ_a). For Region 3, possibilities included an increase in:

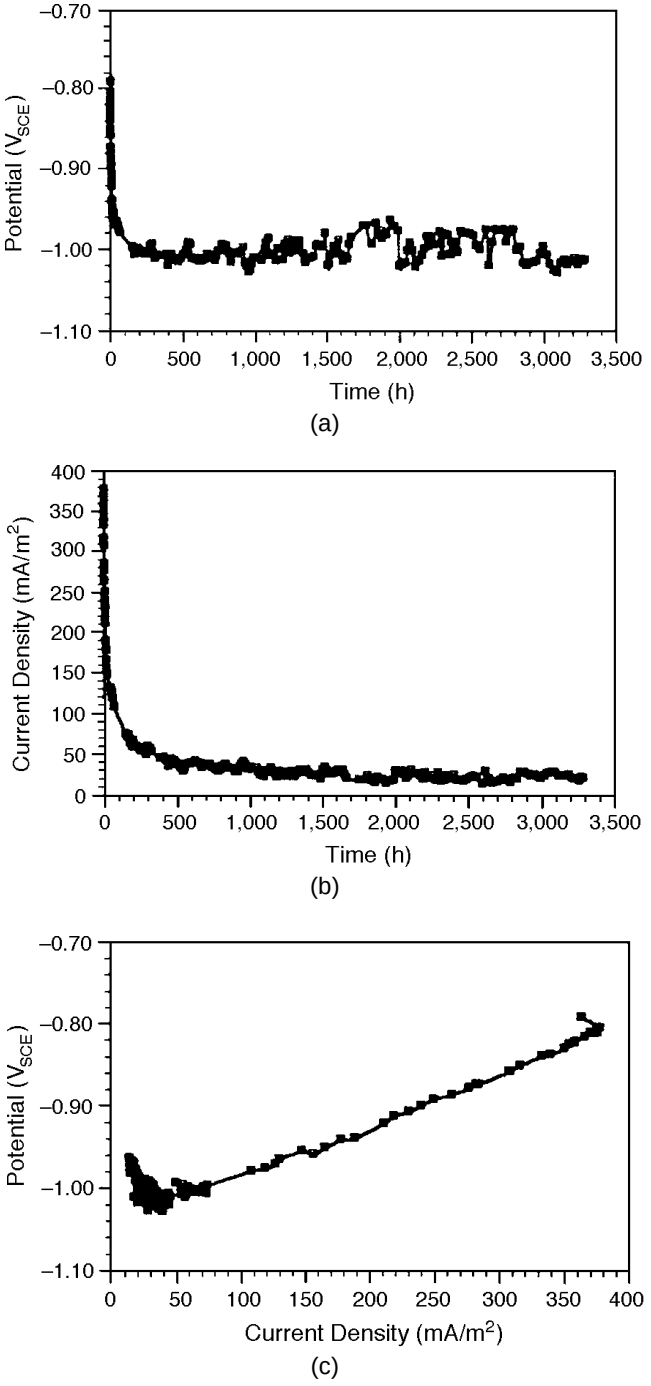


FIGURE 4. *Test results for a specimen with external resistance of 149 Ω: (a) ϕ_c vs time, (b) i_c vs time, and (c) ϕ_c vs i_c.*

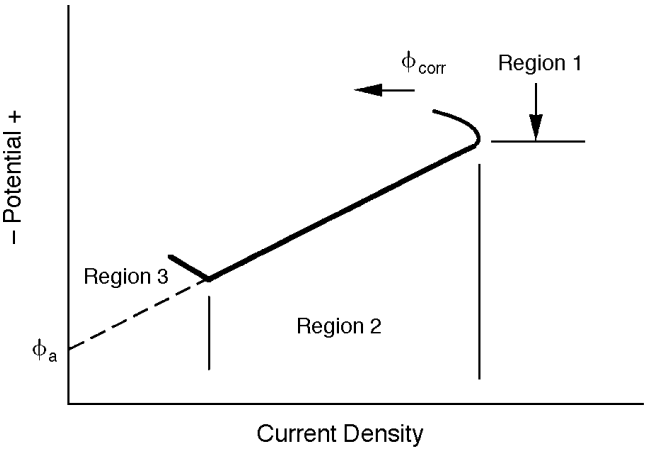


FIGURE 5. *Schematic of the ϕ-vs-i interrelationship for cathodically polarized steel in seawater.*

— Anode resistance with time due to corrosion product accumulation,

— Cathode resistance in association with calcareous deposit formation, and

— Anode potential as a consequence of reduced current output and passivation. Figure 6 presents a plot of the Region 3 ϕ_c and ϕ_a as a function of time. The ϕ_c reported here was measured directly using the SCE reference electrode, whereas ϕ_a was calculated from this by subtracting I_cR_x. Independent measurements of ϕ_a relative to the RE indicated this to be within several millivolts of the calculated value. If either an anode resistance increase with time due to corrosion product accumulation or a cathode resistance increase in association with calcareous deposit formation (or a combination of the two) were responsible for the Region 3 behavior, then this should have been reflected as a time dependence of the slope parameter (R_t x A_c). The increase in the slope parameter necessary to conform to the experimental data would have had to be tenfold, however, meaning that R_a + R_c would have totaled 1,500 Ω.

Limited measurement of these parameters by current interruption in conjunction with a dynamic signal analyzer revealed an upper limit for the former of 72 Ω and for the latter 130 Ω. It was concluded that a linear ϕ-vs-i decay occurs in association with sacrificial-anode CP, at least in the case of the laboratory specimens studied, but that a positive departure from this linearity may result as a consequence of anode passivation if i_a becomes too low. Consistent with this projection, the anode in the test cells typically exhibited localized pitting but with most of the surface being uncorroded.

If anode passivation was responsible for the Region 3 behavior, then an experimental protocol that involves a larger cathode and correspondingly smaller R_x may be more appropriate than what was used for the present experiments. Figure 7 shows the experimental setup whereby a 20.3 cm by 20.3 cm (8 in. by 8 in.) steel plate was coupled to a cylindrical aluminum-zinc-mercury anode (38 mm [1.5 in.] diameter by 32 mm [1.265 in.] length, surface area 49 cm^2 [7.6 in.^{2}]) through a 17-Ω resistor (R_x x A_c = 0.70 Ω-m^2) and exposed to quiescent, once-through seawater. Figure 8 presents the resultant ϕ-vs-i decay diagram. Region 3 is less defined here compared to

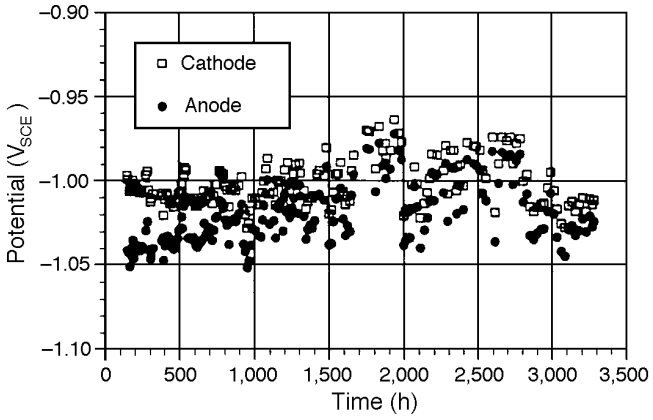


FIGURE 6. *ϕ_c and ϕ_a vs time for specimen with external resistance of 149 Ω (Region 3 of Figure 4).*

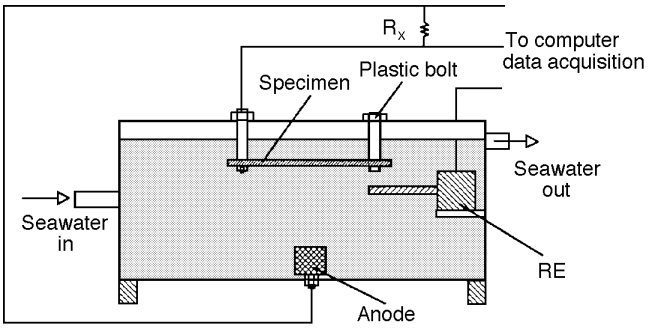


FIGURE 7. *Test cell setup for large plate steel specimen.*

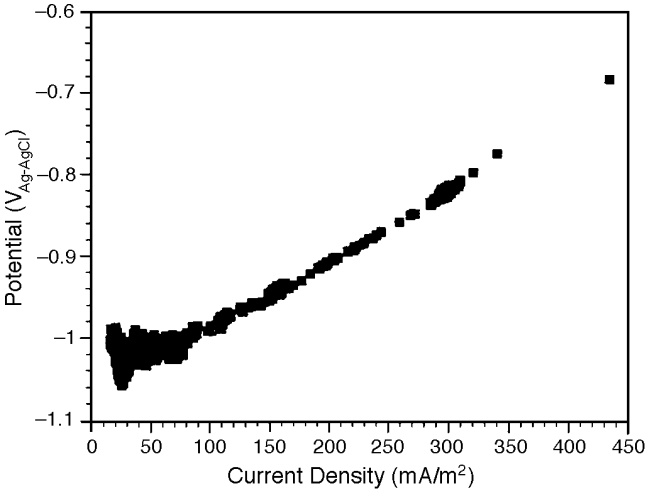


FIGURE 8. *ϕ_c vs i for 20.3-cm (8-in.) square steel plate specimen with external resistance of 17 Ω.*

that in Figure 4(c), with the data appearing essentially as scatter to the positive side of the Region 2 line.

An important consideration for this type of experiment is determination of the most appropriate anode and cathode sizes. Factors to be taken into account include:

— Test cell size and material and electrolyte availability limitations,

— The possibility of anode passivation in association with low current output at long exposure time, and

— Undesired anode performance resulting from compositional inhomogenities in cases where the electrode is acquired from a commercial casting.

Consideration of the first factor leads to a specimen size that is as small as practical. The second factor suggests that a small anode should be specified, although it is the relative surface area difference between the anode and cathode coupled with magnitude of the external resistor that determines current density on the anode. However, avoidance of a difficulty in association with the third factor leads to specification of a relatively large anode surface area.

Hence, the problem of electrode and cell sizing is one of optimization based upon the contrasting role of different influential factors. The data in Figure 4(c) suggest that the electrode sizes here (40.5 cm^2 [6.28 $in.^2$] cathode surface area and 29.8 cm^2 [4.6 $in.^2$] for the anode) were smaller than ideal, while the results in Figure 8 indicated sizes here were an improvement. The long-term anode current density for the former was ~ 20 mA/m^2 and for the latter was 170 mA/m^2.

Figure 9 shows representative ϕ-vs-i decay results from experiments covering the range of external resistances investigated and for exposure times to 3,200 h. The change in the cathodic polarization curve with time is indicated by the dashed lines. The shortest time data (24 h) revealed only limited oxygen concentration polarization but with water dissociation:

$$H_2O + 2e^- \rightarrow H_2 + 2OH^- \quad (6)$$

apparently causing a relatively high current density in the lowest R_x case. Current density decreased as exposure duration increased, however, such that a sigmoidal trend became apparent after 480 h, in agreement with Figure 1. It was confirmed that the slope of a straight line constructed through the individual datapoints for a particular experiment was $\approx R_x \times A_c$. Region 3 behavior was apparent for the lowest long-term current density experiments only ($R_x \times A_c$ = 11.65 Ω-m^2, 15.33 Ω-m^2, and 23.30 Ω-m^2), which was consistent with the projection above that this behavior resulted from anode passivation.

Figure 10 reproduces the long-term data from Figure 9 and illustrates this sigmoidal trend in greater detail.[3] The higher the value for R_x was, the greater the amount of corrosion product on the specimens and the less the amount of calcareous

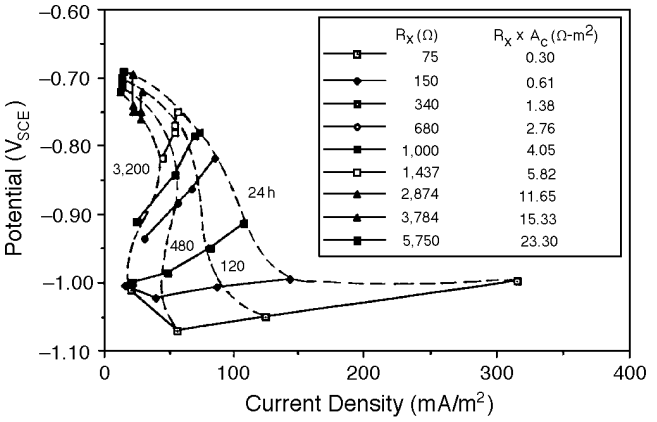


FIGURE 9. *ϕ_c vs i for representative laboratory experiments at different exposure times.*

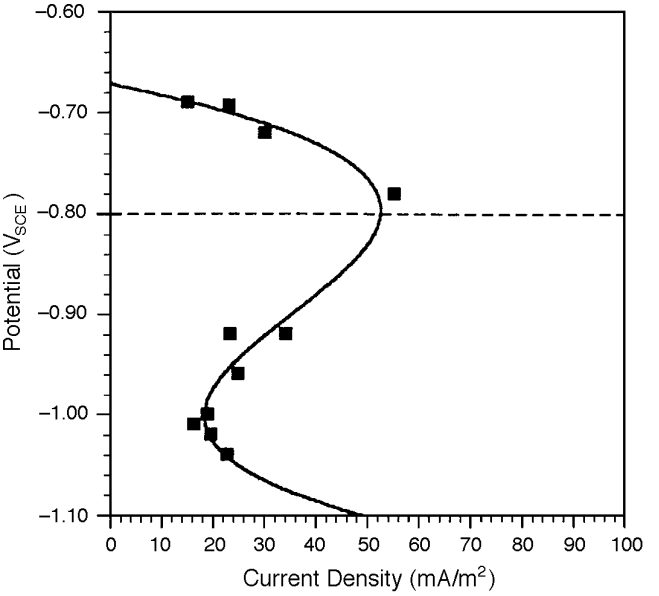


FIGURE 10. *Long-term ϕ_c vs i for laboratory experiments.*

deposits. The current density minimum near –1.00 V_{SCE} was attributed to the calcareous scale that formed under this experimental condition (i.e., the value of the slope parameter for this experiment) being particularly protective. It must be emphasized, however, that the data in Figures 9 and 10 were acquired from ambient temperature, quiescent water experiments; and the steady-state current density likely would have been greater if temperature had been lower or velocity higher.[4,17] Also, the current density for the different experiments appeared to have reached a constant or steady-state value prior to 3,200 h in most cases. However, the timeframe for these laboratory experiments was relatively short compared to what transpires in service. It was possible that further current density decreases might occur after a more extended exposure.

Comparisons with Field Data

Three examples of field data were identified from the literature to permit testing of the appropriateness of Equation (5) and of the linearity of the ϕ-vs-i trend.

North Sea Example — MacKay performed a North Sea exposure of instrumented, single aluminum-zinc-mercury and aluminum-zinc-indium anode-steel couples at depths of –120 m (394 ft) and –180 m (589 ft) to evaluate anode performance.[18] A shunt resistor of 0.012 Ω (R_x) was included for current measurement. Anode resistance was calculated as 0.233 Ω, and cathode surface area was 4.44 m^2 (48.84 ft^2).

Figures 11(a) through (c) present ϕ-vs-time, i-vs-time, and ϕ-vs-i decay curves, as constructed from the reported data. In the last case (ϕ-vs-i decay), the data exhibit an approximately linear trend with a vertical intercept near –1.10 V_{SCE}, and from the value for R_t (0.245 Ω), a slope of 1.09 Ω-m^2 was calculated.

It was determined that an R_x of 270 Ω for the present specimen geometry (A_c = 40.5 cm^2 [6.28 in.^{2}], see Figure 3) resulted in approximately the same value for the slope parameter (R_t x A_c = 1.09 Ω-m^2) as for MacKay's exposures. In Figure 12, the ϕ-vs-i decay for an experiment in the present program with R_x = 268 Ω is compared with MacKay's results from Figure 11(c). This comparison showed good agreement between the two, but with the present data displaced to more positive potentials, apparently because of differences in ϕ_a for the two experiments. This was consistent with the potential for aluminum anodes being more negative in cold water than warm.[19] The measured value for the laboratory data slope parameter was 1.16 Ω-m^2.

Gulf of Mexico Structure: Example 1 — Mateer reported the results of survey data obtained from existing offshore structures where current output from anodes was measured by two independent techniques (potential drop and gauss meter).[20] Figure 13 plots these measured currents vs the corresponding anode-cathode potential difference. The linear interdependence between these two parameters was consistent with what was projected by Equation (5).

Gulf of Mexico Structure: Example 2 — Kennelley and Mateer reported polarization results for a production jacket structure in 162-m (531-ft) Gulf of Mexico water.[21] As a part of the CP system, aluminum-zinc-indium anodes[4] were instrumented for data acquisition at the –37-m (–121-ft) and –105-m

[3] Minor differences are present between the data in these two figures because additional experiments and longer exposure times are included in Figure 10 than in Figure 9.

[4] A limited number of instrumented bimetallic magnesium/aluminum-zinc-indium anodes also were used, but data from these are not addressed here.

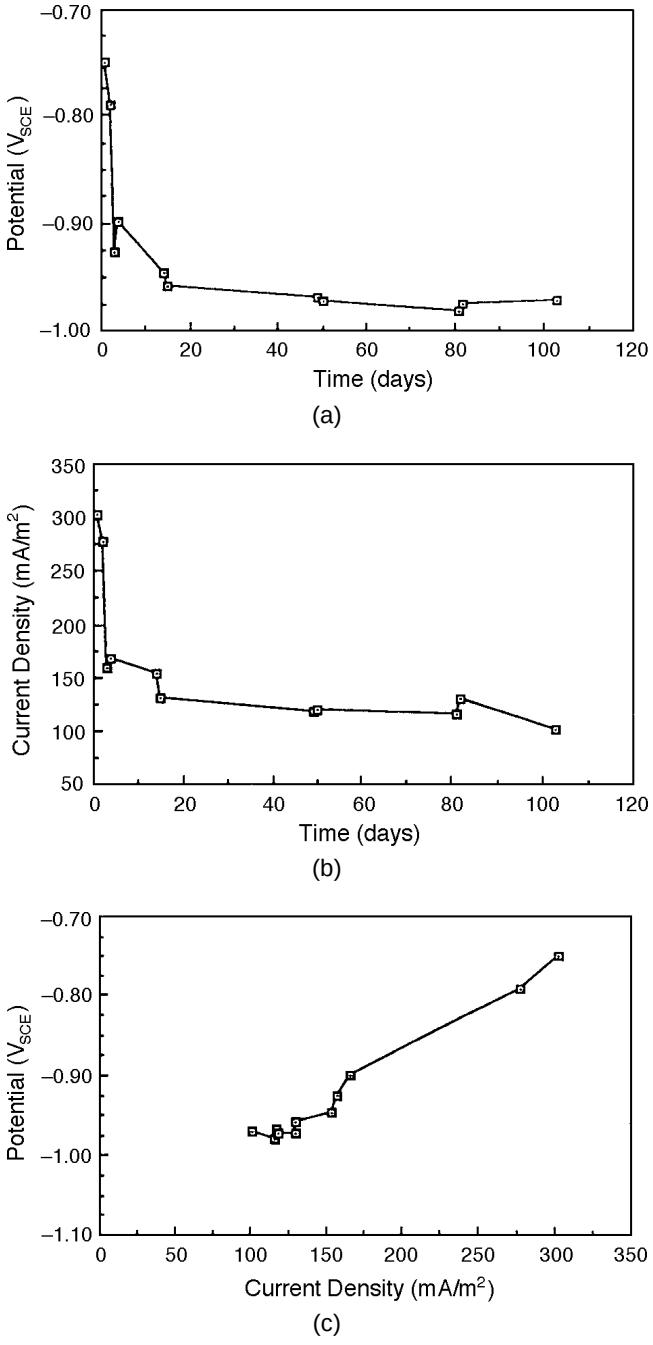


FIGURE 11. *Results from MacKay's[18] experiments: (a) ϕ_c vs time, (b) i_c vs time, and (c) ϕ_c vs i.[18]*

(–344-ft) depths; and potential and current were recorded for the initial 7,000 h of deployment. The CP design parameters were reported as i_o (initial current density[1]) = 280 mA/m^2 and $i_m = i_f$ (final current density[1]) = 65 mA/m^2 with the corresponding number of 330-kg (725-lb) anodes being 265, 216, and 141, respectively. The largest of these three (265 anodes) was used.

For the present laboratory experiments $R_t \cong R_x$ as explained above, whereas for offshore structures, the

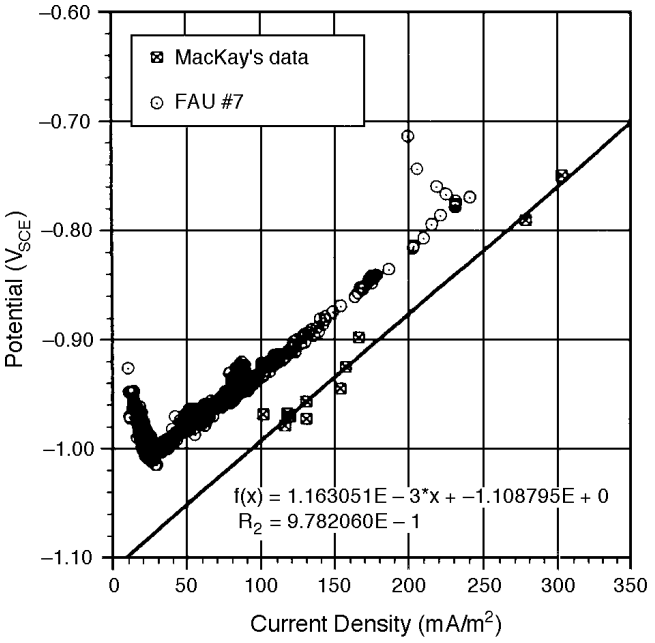


FIGURE 12. *Comparison of field and laboratory polarization data.[18]*

anode resistance dominates and so $R_t \cong R_a$. Thus, in the former case:

$$S = R_x \times A_c \quad (7)$$

where S is the slope parameter, and for the latter:

$$S = \frac{\left(R_a \times A_c\right)}{N} \quad (8)$$

where N is the number of anodes that are intended to protect area A_c. Considering an ϕ_a of –1.10 V_{SCE}, the ϕ-vs-i decay slope for the structure addressed by Kennelley and Mateer was calculated as:

$$\frac{-0.60\ \text{V} - (-1.10\text{V})}{0.280\text{A/m}^2} = 1.79\,\Omega\text{–m}^2 \quad (9)$$

assuming the potential corresponding to the initial current density (280 mA/m^2) was –0.60 V_{SCE}. Because this slope did not closely match any of those from the present set of experiments, an additional laboratory test was performed using an external resistor of 450 Ω ($R_t \cong R_x$ = 1.83 Ω-m^2). Figure 14 plots both sets of data and reveals these to fall on approximately the same straight line.

Figure 14 also indicates that data from the Gulf of Mexico structure extended further along the decay line than did results from the laboratory experiment. This could be attributed either to the fact that the Kennelley and Mateer data were acquired over 7,000 h,

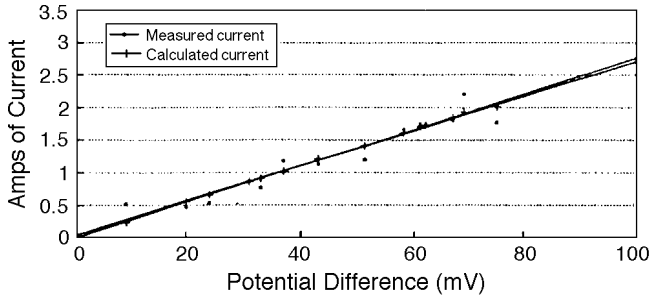


FIGURE 13. *Comparison of calculated and measured anode current output and anode-cathode potential difference on an offshore structure.*[20]

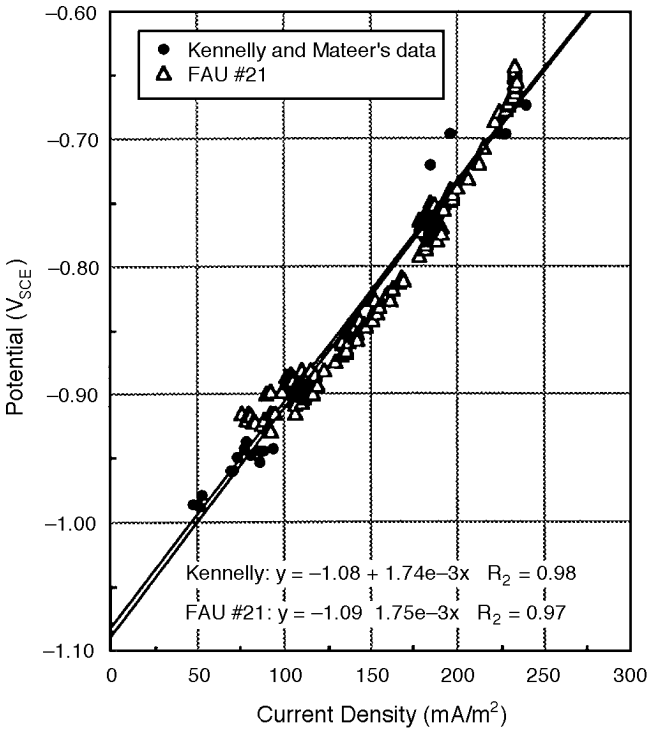


FIGURE 14. *Comparison of Kennelley and Mateer's data to laboratory test results.*[21] *Calculated slope for the field case was 1.79 Ω-m² and for the laboratory experiment was 1.74 Ω-m². (The higher long-term current density for the laboratory data shown here compared to those in Figures 9 and 10 was due to differences in flow rate which, in the case above, was 450 mL/min compared to 150 mL/min.*

whereas the time for the present experiments was 1,400 h. Thus, greater time was available in the former case for calcareous deposit development and associated oxygen concentration polarization. Alternately, a distinction in oxygen availability caused by differences in water composition, flow character, or temperature (or a combination of these) could have been responsible. However, even the 7,000-h current density for the structure was greater than the current density at this same potential (~ –1.00 V_{SCE}) for the long-term laboratory experiments (Figure 10). Also, no Region 3 is apparent for the field data, consistent with the fact that the anode-cathode area ratio here was more extreme than for either of the two laboratory experimental techniques (Figures 3 and 7). Such behavior (occurrence of a Region 3) might result, however, if current density on the structure decreases further and anode passivation occurs.

CONCLUSIONS

❖ The potential and current density of API-2H, grade 42 steel specimens cathodically polarized in seawater by coupling through an external resistor to an aluminum-zinc-mercury anode conformed to a mutually linear interdependence provided the net circuit resistance and ϕ_a were constant with time. The slope of the straight line interrelationship was the product of the total circuit resistance and cathode surface area, and the vertical intercept was ϕ_a. Departures from linearity, which occurred for some experiments after extended exposure times, apparently resulted from low anode current output and associated anode passivation.

❖ An experimental procedure for laboratory and field studies of marine CP was developed that involves connecting a steel cathode through an appropriately sized external resistor to a sacrificial anode. Consideration should be given in sizing the electrodes such that anode passivation does not occur or, if passivation does take place, that any influence upon ϕ_c is discerned.

❖ The long-term, steady-state interdependence between ϕ and i for cathodically polarized steel specimens in seawater conformed to a sigmoidal trend, where a particularly protective calcareous deposit formed near –1.00 V_{SCE} and rendered i_m here minimal.

❖ The same linear interdependence between ϕ and i that described the polarization behavior of laboratory specimens was confirmed also to apply in the case of several offshore structures. This demonstrated that cathodic polarization behavior of specimens and structures of vastly different size can be interrelated through the slope parameter (R_t x A_c).

ACKNOWLEDGMENTS

The authors acknowledge the financial support of Amoco, British Petroleum, Chevron, Elf Aquitaine, Exxon, Mobil, Shell, and Texaco through a joint industry project and assistance from technical representatives from these companies, including J. Burk, S. Byatt, D. Townley, M. Roche, S. Smith, M. Surkein, J. Weeks, S. Wolfson, and R. Lewis. The

anode material was provided by S. Wolfson of Shell Oil Co.

REFERENCES

1. NACE Standard RP0176-92, "Corrosion Control of Steel-Fixed Offshore Platforms Associated with Petroleum Production" (Houston, TX: NACE, 1992).
2. Det Norske Veritas Recommended Practice RP B401, "Cathodic Protection Design" (Hovitz, Norway: Det Norske Veritas Industri Norge AS, 1993).
3. G.C. Cox, "Anticorrosive and Antifouling Coating and Method of Application," U.S. patent 2,200,469 (1940).
4. S.L. Wolfson, W.H. Hartt, Corrosion 37 (1981): p. 70.
5. W.H. Hartt, C.H. Culberson, S.W. Smith, Corrosion 40 (1994): p. 609.
6. S-H. Lin, S.C. Dexter, Corrosion 44 (1988): p. 615.
7. J.E. Finnegan, K.P. Fischer, "Calcareous Deposits: Calcium and Magnesium Ion Concentrations," CORROSION/89, paper no. 581 (Houston, TX: NACE, 1989).
8. K.P. Fischer, J.E. Finnegan, "Cathodic Protection Behavior of Steel in Seawater and the Protective Properties of the Calcareous Deposits," CORROSION/89, paper no. 582 (Houston, TX: NACE, 1989).
9. J.S. Luo, R.U. Lee, T.Y. Chen, W.H. Hartt, S.W. Smith, Corrosion 47 (1991): p. 189.
10. K.E. Mantel, W.H. Hartt, T.Y. Chen, Corrosion 48 (1992): p. 489.
11. T. Foster, V.G. Moores, "Cathodic Protection Current Demand of Various Alloys in Seawater," CORROSION/86, paper no. 295 (Houston, TX: NACE, 1986).
12. S. Evans, MP 27, 2 (1988): p. 9.
13. C.F. Schrieber, J. Reding, "Application Methods for Rapid Polarization of Offshore Structures," CORROSION/90, paper no. 381 (Houston, TX: NACE, 1990).
14. K.P. Fischer, T. Sydberger, R. Lye, "Field Testing of Deep Water Cathodic Protection on the Norwegian Continental Shelf," CORROSION/87, paper no. 67 (Houston, TX: NACE, 1987).
15. S.L. Wolfson, Shell Development Co., Houston, Texas, personal communication.
16. W.H. Hartt, "Fatigue of Welded Structural Steel in Seawater," paper no. 3962, Proc. Offshore Tech. Conf. (Richardson, TX: Soc. Pet. Eng., 1980).
17. M.M. Kunjapur, W.H. Hartt, S.W. Smith, Corrosion 43 (1987): p. 674.
18. W.B. MacKay, MP 13, 8 (1974): p. 36.
19. J.F. Brown, W.J. Engelhard, "KA90 Aluminum Alloy Anodes in Hot and Cold Seawater and Brine Environments," CORROSION/80, paper no. 251 (Houston, TX: NACE, 1980).
20. M.W. Mateer, "Often Overlooked Data Available from a Typical Offshore Subsea Survey," CORROSION/91, paper no. 233 (Houston, TX: NACE, 1991).
21. K.J. Kennelley, M.W. Mateer, "Evaluation of the Performance of Bimetallic Anodes on Deep-Water Production Platform," CORROSION/93, paper no. 523 (Houston, TX: NACE, 1993).

